

Product, process, property, and performance (PPPP) relationship of 3D-Printed polymers and polymer composites: Numerical and experimental analysis

Ans Al Rashid, Shoukat Alim Khan, Muammer Koç

Item type

Journal Contribution

Terms of use

This work is licensed under a [CC BY-NC-ND 4.0](https://creativecommons.org/licenses/by-nc-nd/4.0/) license

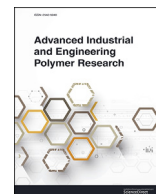
This version is available at

https://manara.qnl.qa/articles/journal_contribution/Product_process_property_and_performance_PPPP_relationship_of_3D-Printed_polymers_and_polymer_composites_Numerical_and_experimental_analysis/26354836/1

Access the item on Manara for more information about usage details and recommended citation.

Posted on Manara – Qatar Research Repository on

2024-04-18



Research paper

Product, process, property, and performance (PPPP) relationship of 3D-Printed polymers and polymer composites: Numerical and experimental analysis

Ans Al Rashid^{*}, Shoukat Alim Khan, Muammer Koç

Division of Sustainable Development, College of Science and Engineering, Hamad Bin Khalifa University, Qatar Foundation, Doha 34110, Qatar

ARTICLE INFO

Article history:

Received 14 November 2023

Received in revised form

4 December 2023

Accepted 6 December 2023

Keywords:

Additive manufacturing

Fused filament fabrication

Numerical model

Process simulation

Mechanical testing

ABSTRACT

Understanding the external and internal factors during an additive manufacturing (AM) process is crucial, as they can significantly affect the final product's performance. Efforts have been made to unwind the product, process, property, and performance (PPPP) relationships. The conventional experimental approaches can lead to boundless runs, resulting in exorbitant costs for research and development. Hence, developing, adapting, and validating numerical models is essential to achieving the desired performance of 3D-printed products with lesser resource utilization. In this study, numerical and experimental techniques were used to perform the PPPP relationship assessment on material extrusion 3D-printed parts. Three infill designs (rectangular, triangular, and hexagonal), with layer heights (0.1 mm, 0.125 mm, and 0.2 mm), and three different materials (carbon fiber-reinforced polyamide-6 (PA6-CF), polyamide-6 (PA6), and acrylonitrile butadiene styrene (ABS)), were selected for the investigation. Taguchi's design of experiments (DOE) method was used to limit the number of numerical simulations and experimental runs. A thermomechanical numerical model was utilized to perform the material extrusion process simulations and mechanical performance prediction of the specimens. Subsequently, the samples were 3D-printed and tested mechanically to validate the numerical simulation results. The dimensional, distortion, and mechanical analysis performed on numerical simulation results agreed well with the experimental observations.

© 2023 Kingfa Scientific and Technological Co. Ltd. Publishing services by Elsevier B.V. on behalf of KeAi Communications Co. Ltd. This is an open access article under the CC BY-NC-ND license (<http://creativecommons.org/licenses/by-nc-nd/4.0/>).

1. Introduction

The fused filament fabrication (FFF) technique is the most widely explored and adopted additive manufacturing (AM) or 3D printing (3DP) process for polymers and polymer composites [1–4]. Owing to the flexibility and inexpensive availability of FFF-based 3D printers, these processes are recent research and development interest for several industries [5]. In this process, a viscous material (generally polymers) is extruded through a heated nozzle and laid over a printing bed in a layered manner to achieve three-dimensional (3D) objects [6]. Although the process seems straightforward, plenty of internal and external factors determine the quality of the final part [7]. Therefore, understanding the

interlinkages of product design (forms, shapes, topology, surface texture), process (speed, temperature, resolution, principle), and property (base material, porosity, reinforcement type, content) is crucial, which ultimately affects the performance (robustness, response, quality, dimensional control) of 3D-printed parts [8], as shown in Fig. 1.

Different polymeric materials have been explored for FFF processes to investigate their performance and to optimize the 3DP process parameters. For instance, N. Vidakis et al. [9] investigated the impact of multiple recycling on the mechanical properties of acrylonitrile-butadiene-styrene (ABS) polymer for the FFF 3DP process. Tensile, compression, flexural and micro-hardness tests were performed for each recycling succession. The results revealed an improved mechanical response of ABS polymer with the recycling process with an optimum mechanical behaviour achieved at the third and fifth recycling replications. N. Vidakis et al. [10] explored the potential of using silver-doped antibacterial nanopowder (AgDANP) as a reinforcement to polyamide 12 (PA12) for

^{*} Corresponding author.

E-mail addresses: aalrashid@hbku.edu.qa (A. Al Rashid), mkok@hbku.edu.qa (M. Koç).

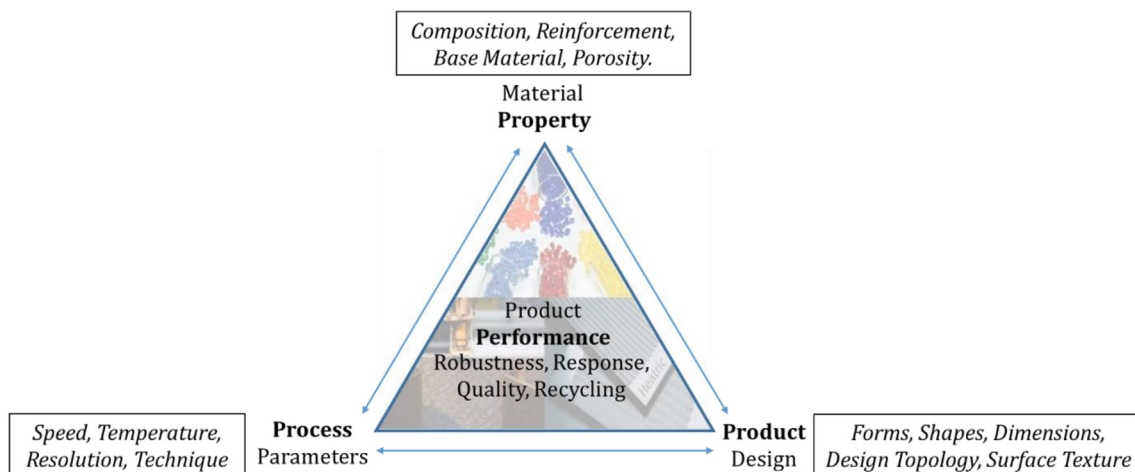


Fig. 1. Product, process, property, and performance (PPPP) linkages of the 3D-Printed parts.

producing medical equipment. Different concentrations of AgDANPs were used to synthesize nanocomposites and microscopic, mechanical, and antibacterial assessments were performed. Results revealed around 27 % improvement in the tensile and flexural performance of the nanocomposites at two wt% concentration of AgDANPs, with a high antibacterial performance. In another study, N. Vidakis et al. [11] developed a facile process to produce nanocomposites for material extrusion 3DP process. Silver nitrate was used as a reinforcement and antibacterial agent to PA12 to synthesize PA12/Ag nanocomposites via a reactive melt mixing process. Polyethylene glycol (PEG) and polyvinylpyrrolidone (PVP) were used as reduction agents. The resulting nanocomposites revealed an improved mechanical response and antibacterial performance at 5 wt% loading of silver nitrate and 2.5 wt% of PEG.

C. David et al. [12] optimized energy efficiency and compressive behaviour for the material extrusion process of polyamide 6 (PA6). Different processing parameters were studied, including layer height, printing temperature, printing speed, bed temperature, etc. Layer height was the most significant parameter of energy consumption and printing time, while compressive strength was highly dependent on the infill density of specimens. M. Petousis et al. [13] optimized energy efficiency and compressive behaviour for the material extrusion process of ABS. Layer height was the most significant parameter; however, printing temperature and raster angle were less significant. N. Vidakis et al. [14] demonstrated the impact of strain rate under static loading conditions for 3D-printed parts fabricated using different polymeric materials, i.e., polylactic acid (PLA), ABS, polyethylene terephthalate glycol (PETG), PA6, and polypropylene (PP). PA6, ABS, PETG, and PP were observed to be less sensitive to strain rates; however, PLA revealed a higher sensitivity to strain rates. N. Vidakis et al. [15] synthesized multi-wall carbon nanotubes (MWCNT) reinforced PA12 composites for improved electrical and mechanical properties. A melt mixing process was used to produce nanocomposites at different concentrations of MWCNTs. Improved thermomechanical properties were observed at 5 wt% of MWCNTs loading; however, increased electrical conductivity was revealed with increased nanoparticle concentrations.

Warp and distortions during the material extrusion processes for polymers have also been under investigation. J. Ramian et al. [16] evaluated the distortions (warp) for ABS polymer during the FFF process. A thermal camera was used to analyze the thermal distributions during the 3DP process, and 3D-printed samples were scanned using a 3D scanner for comparison with the

designed parts. Based on the results, it was concluded that the bigger surface area should be parallel to the print bed to avoid detaching and cracks. Secondly, the printing and print bed temperatures should be selected based on the material grade to avoid warpages and distortions. N. Yu et al. [17] developed a modified 3D printer with an auxiliary heating plate mounted on the print head to minimize the warpages in the carbon fiber (CF) reinforced ABS composites. Due to the annealing phenomena, the auxiliary heating plate played a vital role in reducing/eliminating the warpages in the 3D-printed parts, resulting in improved mechanical properties. N. Vidakis et al. extensively investigated the impact of different material extrusion processing parameters on dimensional control, roughness, and porosity of ABS [18] and PLA [19] 3D-printed parts. Different sophisticated tools, such as optical microscopy, profilometry and micro-computed tomography (μ -CT), were employed to evaluate these attributes.

As evident from the literature, efforts have been made to unwind the product, process, property, and performance (PPPP) relationships [20–24]. However, the conventional experimental approaches can lead to boundless runs, resulting in exorbitant costs for research and development. Therefore, several computational modeling models have been developed to approximate the material flow behavior, residual stresses, and solidification process [25–36], as well as to predict the mechanical response of 3D printed structures [37–41]. Although literature exists in this field, the reported studies consider only a single sub-process of the FFF process. Secondly, the experimental validations of the computational modeling approaches are limited. A. Al Rashid & M. Koç [42] developed a numerical model to estimate the process-induced defects and warpages during the FFF 3DP process for two polymeric materials, i.e., PA6 and ABS. In another study, A. Al Rashid & M. Koç [43] utilized the same numerical model to evaluate the impact of process parameters on process-induced defects and warpages during the FFF 3DP process. The authors also investigated the impact of different infill designs and densities on the thermo-mechanical performance of 3D-printed parts [44,45]. The results from their studies revealed a sound approximation of distortions (warp) and dimensional accuracy of the 3D-printed parts. However, the combined effect of different materials, process parameters, and specimen geometry is not addressed, as these variables are interconnected and ultimately affect the 3DP process and product performance.

Given the existing literature and research trends in this field, developing, adapting, and validating numerical models is essential

to achieving the desired performance of 3D-printed products with less resource utilization. Therefore, this study uses numerical and experimental approaches to perform the PPPP relationship and sustainability assessment on FFF 3D-printed parts. Considering the complexity of the subject, the design of experiments (DOE) technique was used to limit the numerical and experimental runs. Three different materials (carbon fiber-reinforced polyamide-6 (PA6-CF), polyamide-6 (PA6), and ABS), infill designs (rectangular, triangular, and hexagonal), with layer heights (0.1 mm, 0.125 mm, and 0.2 mm) were selected for the investigation. The presented work is divided into two sections.

- i. The numerical simulation of the FFF process and prediction of mechanical properties with predicted warpage and residual stresses.
- ii. FFF fabrication of specimens, their dimensional and distortion analysis, and tensile testing.

2. Methodology

This study aims to observe the effect of the product (infill design), process (layer height), and property (material) on the performance characteristics (dimensional control and mechanical properties) of additively manufactured parts. The tensile testing coupon was selected as the reference geometry and designed using Solidworks® as per ASTM D638-I [46]. The STL geometry of the designed specimen was imported to slicing softwares, Cura® and Eiger® to define the manufacturing parameters and obtain the toolpath for all the samples. The infill density was kept consistent (50 %) for all the infill patterns, and a visual representation of specimen infills obtained from Eiger software is reported in Fig. 2.

The overall methodology adopted for this study is presented in a graphical abstract. The reported work is mainly divided into two main sections. In the first step, a thermomechanical numerical model was used to perform the FFF process simulations to predict the process-induced warpages and residual stresses. The dimensional analysis was performed on the numerically simulated 3D-printed parts, and the targeted dimensions of the designed parts were measured. The warped geometries with estimated residual stresses were used to predict the mechanical behaviour of the 3D-printed samples numerically. In the second step, the specimens were fabricated using the FFF process. Dimensional measurements were recorded and compared with the numerical model predictions. The 3D-printed parts were tested mechanically under

tensile loading conditions, and numerically predicted mechanical properties were validated.

2.1. Design of experiments (DOE)

The design of experiments (DOE) approach was used to limit the number of experimental and numerical simulation runs. Three different materials (PA6-CF, PA6, and ABS), infill designs (rectangular, triangular, and hexagonal), with layer heights (of 0.10 mm, 0.125 mm, and 0.20 mm) were selected for the investigation. PA6-CF filaments were purchased from Markforged, United States [47], while PA6 and ABS filaments were procured from Ultimaker, Netherlands. In the reported literature, infill designs among the specimen geometry [45] and layer heights among the process parameters [43] were found to be significant parameters affecting the 3DP process performance (dimensional accuracy and distortions) and mechanical behaviour of 3D-printed parts; therefore, they were selected for investigation in this study. Taguchi's DOE approach with three-factor and three-level was used within Minitab® software (Minitab, Inc). Taguchi's L9 (3^3) orthogonal array experimental design reduced the total combinations to 9 runs. Details on Taguchi's design for selected material, specimen design, and layer height are reported in Table 1.

2.2. Numerical simulations

2.2.1. FFF process simulations

The numerical simulations were performed within the Digimat-AM® module of the Digimat® software. The numerical model utilized for the 3DP process simulations is reported elsewhere [42]; readers are referred to section 2 of this study for further details. The 3D printer specifications, type of analysis, process parameters, and simulation details need to be defined for the FFF process simulations. A generic FFF 3D printer was selected with a moving build platform and a build volume of 320 mm × 132 mm × 154 mm and 215 mm × 215 mm × 300 mm in XYZ directions, respectively, as per specifications of Markforged Mark Two® and Ultimaker 3 Extended® used for the 3DP process. Subsequently, the STL geometry of the designed geometry was loaded with toolpath information related to each specimen, and material properties for the selected materials (PA6-CF, PA6, and ABS) were assessed from the Digimat-MX® material database. The extrusion and build plate temperatures were selected based on the literature and are

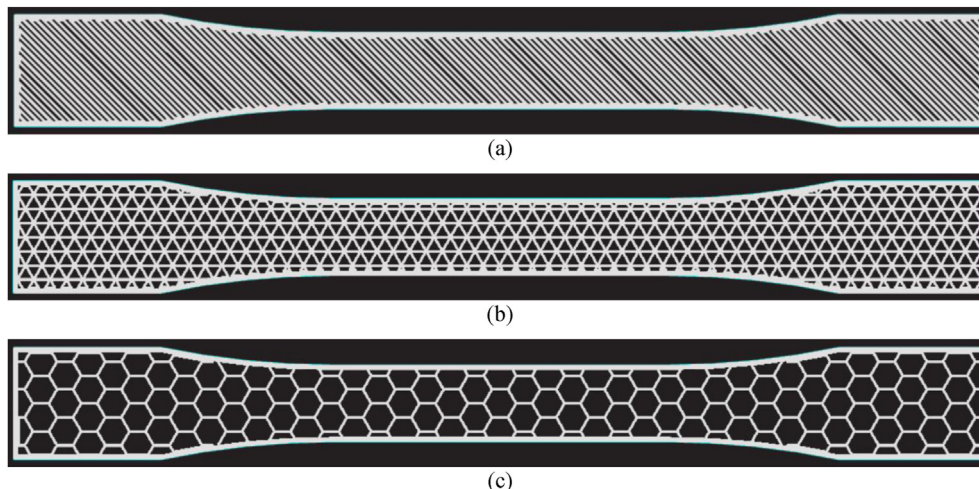


Fig. 2. Three infill patterns designed at 50 % infill density (a) rectangular (b) triangular (c) hexagonal.

Table 1

Taguchi's design of experiments (DOE), 3D printer specifications, and process parameters.

Run	Material	Design	Layer Height	3D Printer	Build Volume (mm ³)	Extrusion Temperature	Build Plate Temperature
1	PA6-CF	Rectangular	0.100	Markforged Mark Two	320 x 132 x 154	275 °C	30 °C
2	PA6-CF	Triangular	0.125				
3	PA6-CF	Hexagonal	0.200				
4	PA6	Rectangular	0.125	Ultimaker 3 Extended	215 x 215 x 300	245 °C	60 °C
5	PA6	Triangular	0.200				
6	PA6	Hexagonal	0.100				
7	ABS	Rectangular	0.200			240 °C	80 °C
8	ABS	Triangular	0.100				
9	ABS	Hexagonal	0.125				

reported in Table 1. The maximum element size of 3.93 mm, bead width of 0.4 mm, ambient temperature of 25 °C, and convection coefficient of 0.015 mW/mm²°C were consistent for all the specimens. The Digimat® software provides two discretization approaches: layer-by-layer and filament. The layer-by-layer finite element activation approach was used to reduce computational time and cost. The voxel sizes of 0.1 mm, 0.125 mm, or 0.2 mm were used based on the experiment performed per the DOE matrix. The same procedure was adopted for all the DOE runs.

2.2.2. Mechanical testing simulations

The warpage and residual stress predictions for all the samples from the FFF process simulations were used in this step to investigate the mechanical behavior numerically. The Digimat-RP® module was used to evaluate the mechanical response of the specimens under tensile loading conditions. An FEA input file was generated using Abaqus® software, where a CAD model of the tensile testing coupon was imported to define the step, loading, and boundary conditions and mesh. The displacements and rotations were fixed to zero at one end of the sample, while displacement along the specimen length was applied at the other end, corresponding to the stationary grip and crosshead movement, respectively. An 8-node brick element with reduced integration (C3D8R) with a global mesh size of 1 mm was used to mesh the sample. Finally, an FEA input file was exported to be used in Digimat-RP®. Besides the input file, the Digimat-RP® requires material properties (imported from the Digimat-MX® material database), toolpath information (from G-codes generated), residual stress, and warpage (from Digimat-AM® numerical simulation results) information. The imported material properties, toolpath, residual stress, and warpage information were embedded in the FEA input file to account for AM process-induced defects and porosity. Finally, the job was submitted for analysis, and the same procedure was adopted for all nine DOE matrix runs. After the successful mechanical

analysis, the strain vs. stress data was imported for further processing.

2.3. FFF experiments

2.3.1. FFF process

The specimens were 3D-printed utilizing two different hardware; Markforged Mark Two® for PA6-CF and Ultimaker 3 Extended® for PA6 and ABS samples, as shown in Fig. 3. The same G-codes used for the numerical simulations were used to fabricate the specimens. All other process parameters used in the numerical simulations were kept the same to ensure consistency. At least three samples were fabricated for each DOE run. The dimensional analysis was performed on the 3D-printed samples to compare and validate the numerically predicted shrinkage and warpages. The dimensional variances and distortions of the 3D-printed samples were analyzed. An overall length, grip width, gauge width, and thickness measurements were conducted using a vernier calliper, whereas warpage was observed through optical microscopy. The recorded dimensions obtained from numerical model predictions and experimental measurements were post-processed for analysis.

2.3.2. Mechanical testing

After the dimensional analysis of the specimens, mechanical testing under tensile loading conditions was performed. The Zwick Roell Z100® universal testing machine (UTM) equipped with a 100 kN load cell and laser extensometer was used for mechanical characterization. Fig. 4 shows the PA6 material sample gripped for mechanical testing. A 5 mm/min test speed was selected, and at least three samples were tested for each DOE run, as per ASTM standard D638. TestXpert III® software (from Zwick/Roell) was used to acquire the experimental data, and results were exported for comparison with numerical model predictions.

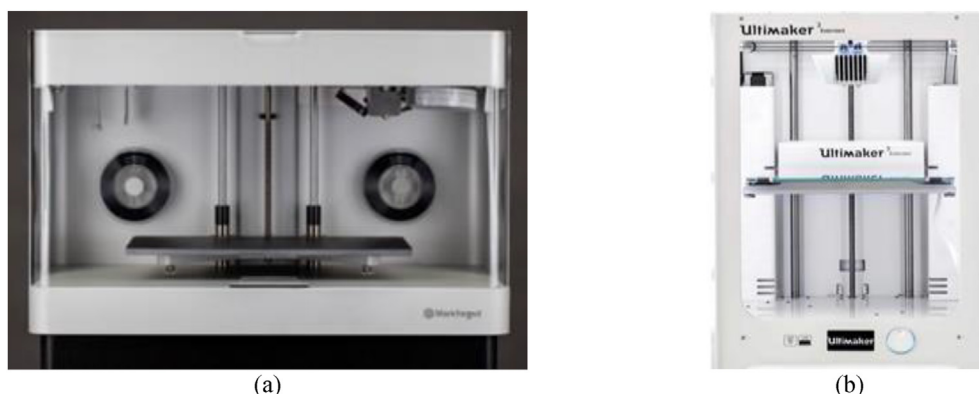


Fig. 3. 3D printers used in this study (a) Markforged Mark two (for PA6-CF) (b) Ultimaker 3 extended (for PA6 & ABS).

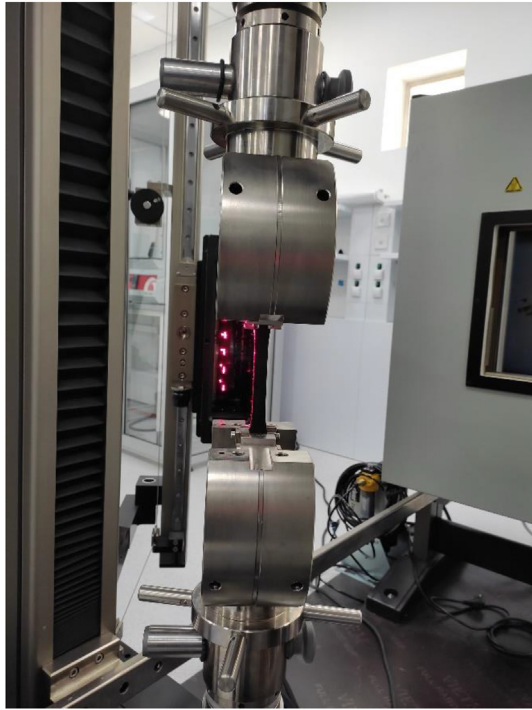


Fig. 4. PA6 sample gripped in universal testing machine (UTM) for tensile testing.

3. Results and discussions

3.1. Dimensional and warpage analysis

After completing the FFF process simulations, the dimensional and warpage analysis was carried out on the numerical model

predictions. The warped geometries were exported in STL format from Digimat-AM® and imported to Solidworks® for dimensional measurements, and targeted dimensions were also measured for the 3D-printed specimens, as shown in Fig. 5. The recorded measurements are reported in Table A1 and graphically presented in Fig. 6. Generally, a good agreement between numerical model predictions and experimental measurements was observed. The numerical model predicted higher shrinkages in all the principal directions, resulting in higher dimensional variations from the targeted dimensions than were physically measured. However, the effect of material properties, design, and layer heights was well captured on the product performance (in terms of dimensional accuracy).

Regarding material properties, PA6-CF provided the best dimensional control of selected measurements, followed by ABS and PA6, respectively. Incorporating short carbon fibers (CFs) into PA6 significantly improves the dimensional control of the 3D-printed parts, as CFs improve the structural integrity and hinder the material shrinkages during the cooling process [48]. In addition, higher control over dimensions was observed at the layer height of 0.100 mm, followed by layer heights of 0.125 mm, and higher variations in dimensions were achieved at 0.200 mm. The 3DP process resolution significantly improves the material deposition control and dimensional accuracy at lower layer heights [49]. The material properties and layer height selection mainly drove the product performance in terms of measurements and reproducibility. Although the choice of infill design and density plays a vital role in the final product quality [44], it was found to be the least significant in this case.

The warpages/distortions analysis was also conducted alongside the dimensions. In this case, the numerical model predicted lower warpages than experimental observations. Higher warpage values were observed for the PA6 material, followed by ABS, and PA6-CF provided the lower distortions. Higher shrinkages and lower distortions observed in the numerical simulation results are attributed

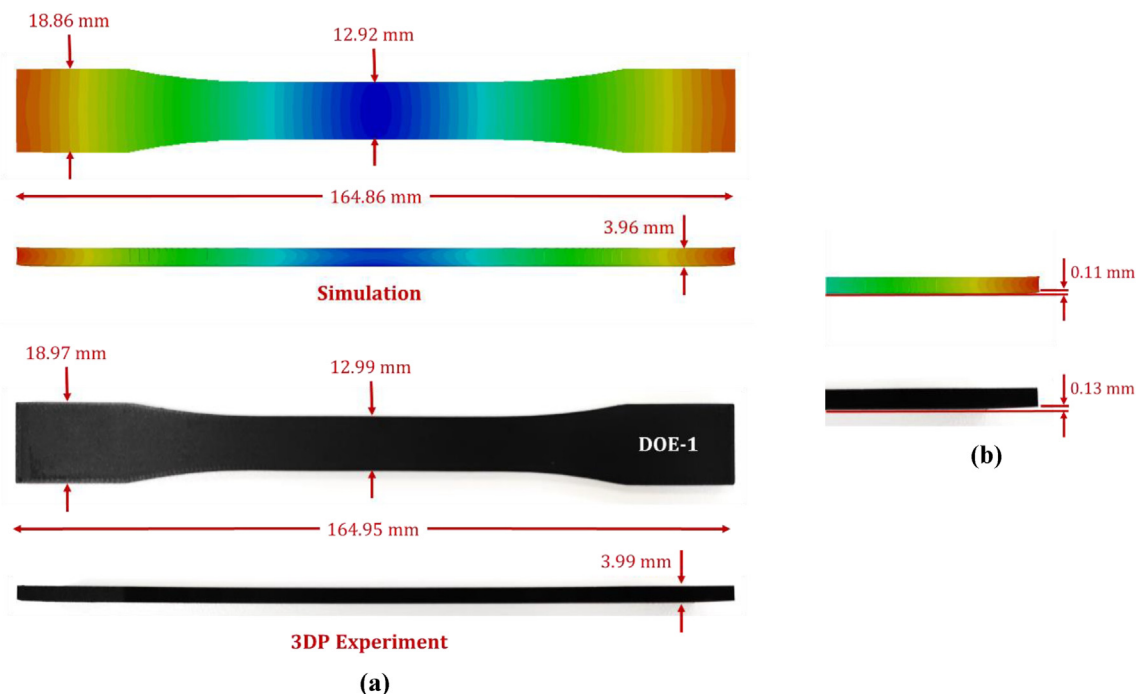


Fig. 5. Measurement of targeted dimensions for numerical model predictions and 3D-Printed Specimens. (a) dimensional (b) warpage analysis.

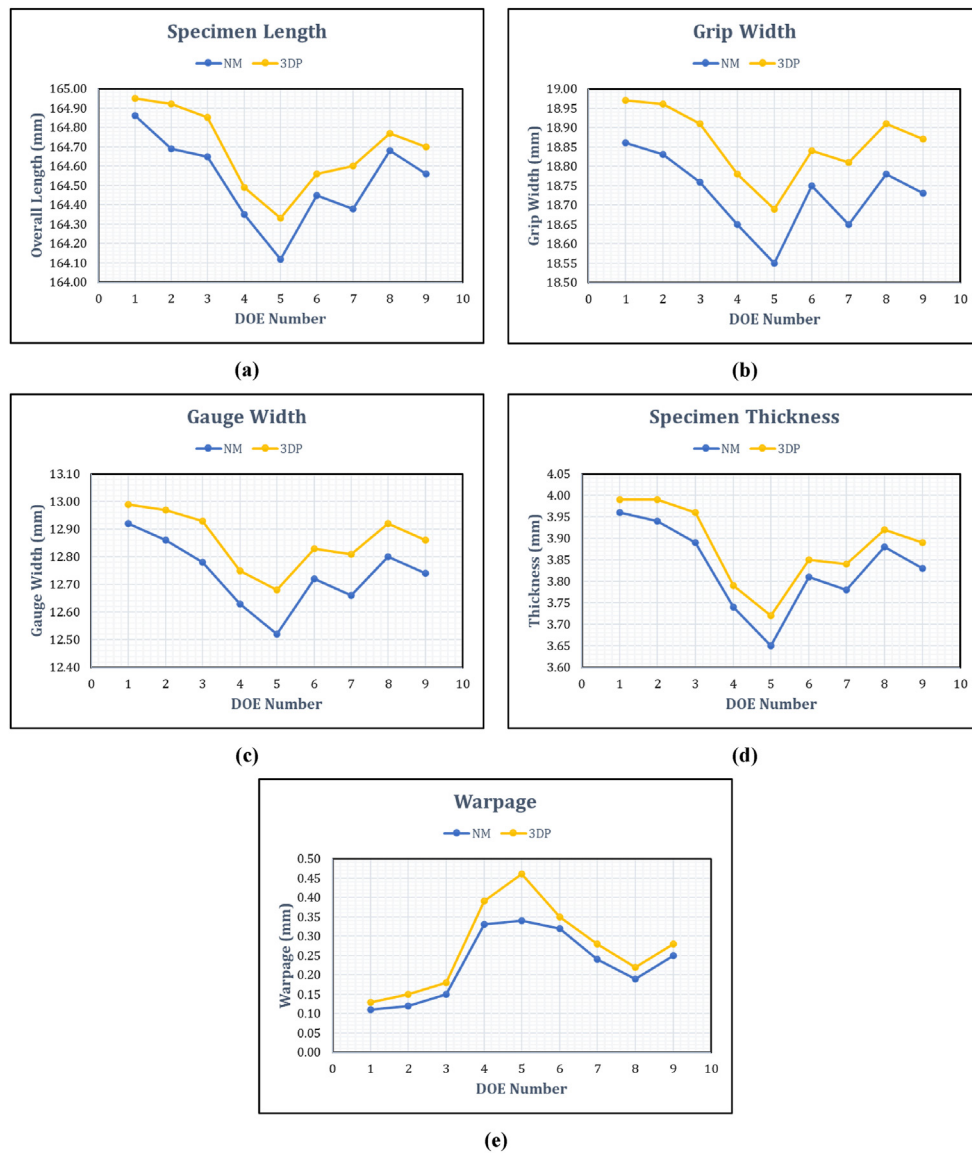


Fig. 6. Targeted Dimensions Observed in Numerical Model (NM) Predictions and 3D-Printed (3DP) Specimens (a) Overall length (b) Grip Width (c) Gauge Width (d) Thickness (e) Warpage.

to the numerical model limitations. The numerical model currently does not consider the stress relaxation phenomena, which reduces the residual stress, and ultimately, the shrinkages are over-predicted [43]. In the case of warpages/distortions, the numerical model assumes the perfect build plate adhesion, resulting in lower distortions; however, during the 3DP process, the imperfect build plate adhesion results in higher warpages [43].

For multiple-factor and multiple-level problems, it is vital to consider the impact of all the variables on the output performance [50]. From the interaction of three variables considered in this study, it is concluded that optimum dimensional control was achieved for PA6-CF material with a rectangular infill pattern fabricated at 0.100 mm of layer height. Conversely, the maximum deviation from the designed values was observed for PA6 material with a triangular infill pattern manufactured at 0.200 mm layer heights. This observation was consistent for all the measured dimensions, i.e., overall length, grip width, gauge width, thickness, and warpage.

3.2. Mechanical response

The strain vs stress response of the 3D-printed samples was obtained through numerical simulations and tensile testing experiments. The mechanical behaviour of the specimens was post-processed to get Young's modulus, yield stress, strain at yield point, and maximum stress. The mechanical properties from numerical model predictions and 3D-printed specimens are reported in Table A2 and graphically presented in Fig. 7. The numerical model adequately predicted the mechanical behavior of the samples, as validated by the experimental observations. Generally, better mechanical properties (Young's modulus, yield stress, and maximum stress) were achieved for ABS material; however, PA6 material revealed higher yield strain. The effect of the infill pattern was not found to be very impactful on the mechanical properties of all the materials and layer heights. The layer heights impacted the mechanical performance of the 3D-printed specimens for PA6-CF and ABS material; however, they were insignificant in the case of PA6

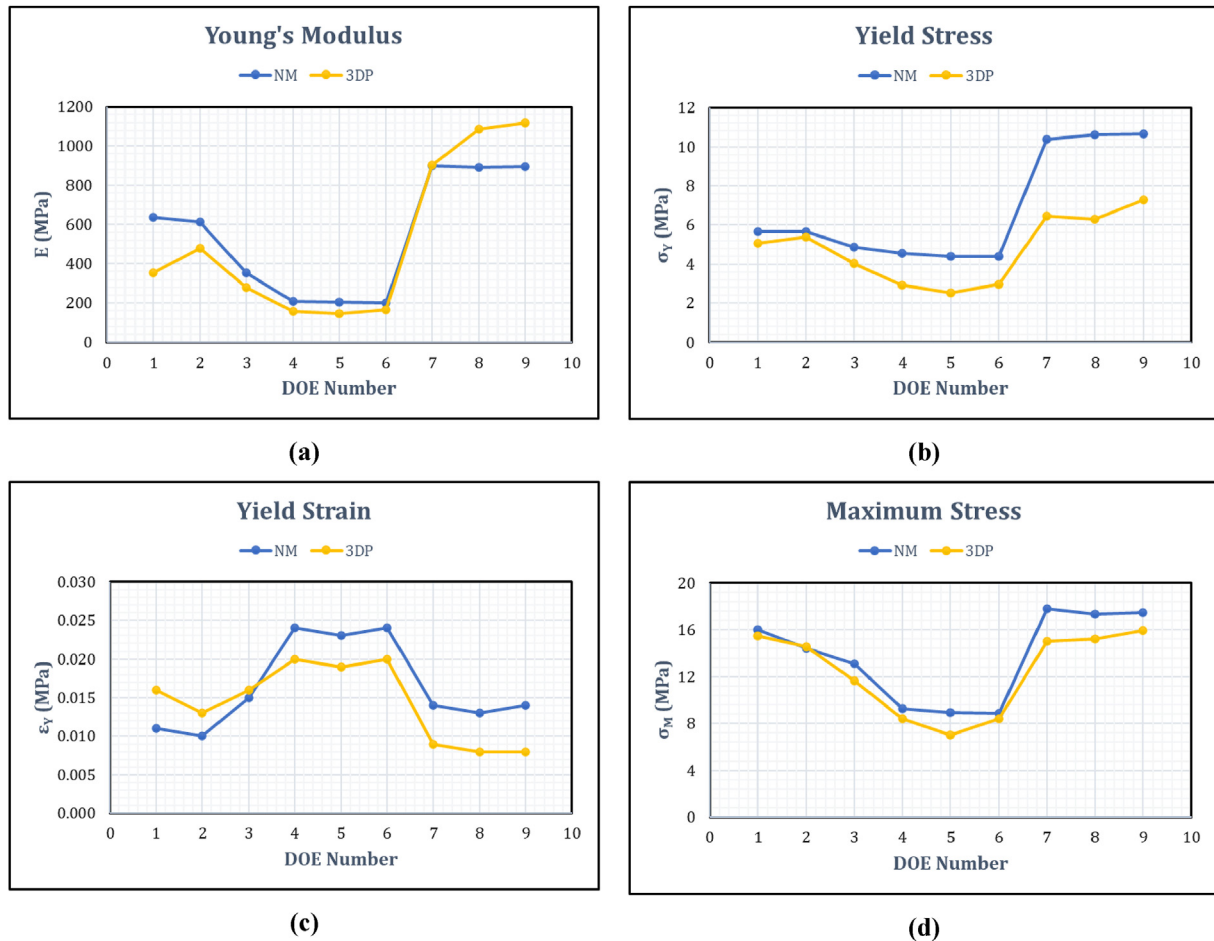


Fig. 7. Mechanical properties in numerical model (NM) predictions and 3D-Printed (3DP) Specimens. (a) Young's modulus (b) yield stress (c) yield strain (d) maximum stress.

material. The numerical simulation for tensile testing also captured the specimen breakage, and it is worth noting that the numerical prediction accurately predicted the material failure during the loading. A comparison of numerical testing results acquired from ABAQUS® and 3D-printed samples after rupture is reported in Fig. 8.

The material properties were the most significant parameter affecting the mechanical performance from numerical model predictions, where ABS provided maximum Young's modulus followed by PA6-CF and PA6, respectively; however, the infill patterns and layer heights did not have a significant effect. 3D-printed

specimens revealed that the maximum Young's modulus was achieved for ABS material with a hexagonal infill pattern fabricated at 0.125 mm of layer height. Similar trends were observed for the yield strength and maximum stress, except for the strain at yield. A maximum strain at yield was observed for PA6 material for rectangular and hexagonal infill patterns fabricated at layer heights of 0.100 mm or 0.125 mm.

Overall, ABS material provided better mechanical performance (Young's modulus, yield strength, and maximum stress); however, maximum strain at yield is recorded for PA6 material. This observation is consistent with the literature, as the ABS material exhibits

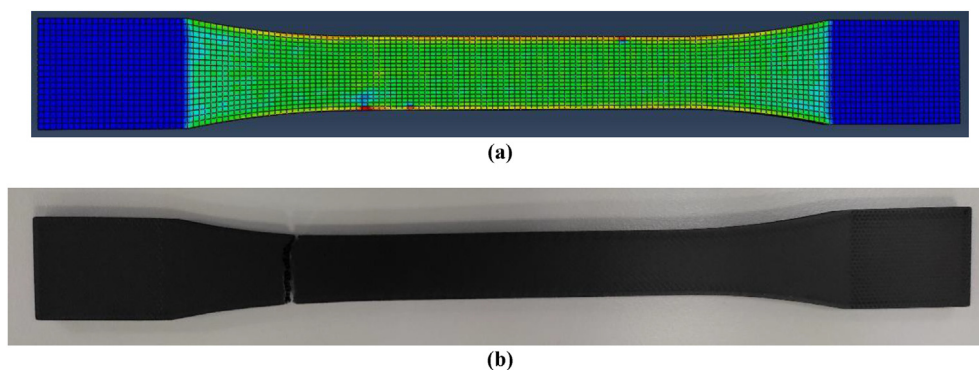


Fig. 8. A comparison of specimen failure for PA6-CF specimen (DOE 1) (a) numerical model (b) 3DP.

excellent mechanical properties [51], and the PA6 material comprises flexible polymer chains with exceptional elasticity [52]. Adding CFs to PA6 material significantly improves its mechanical performance [53]; however, the CFs limit the elongation of polymeric chains, resulting in a lower strain at yield for PA6-CF material [54].

4. Conclusions

This study uses numerical and experimental approaches to assess the PPPP relationship on FFF 3D-printed parts. Considering the complexity of the subject, the DOE approach was used to limit the numerical and experimental runs. Three different materials (PA6-CF, PA6, and ABS), infill designs (rectangular, triangular, and hexagonal) with layer heights (0.1 mm, 0.125 mm, and 0.2 mm), were selected for the investigation. The numerical simulations were performed in two steps; first, the FFF process simulations were conducted to predict the overall part dimensions and distortions following the prediction of mechanical behavior considering the process-induced defects. The 3DP experiments were performed to evaluate the dimensional control and warpages of 3D-printed parts and were mechanically tested. Overall, a sound approximation of dimensions and mechanical performance was achieved from the numerical model predictions, as validated by the experimental results. The numerical model predicted higher shrinkages in all the principal directions, resulting in higher dimensional variations from the targeted dimensions than were physically measured. Higher shrinkages and lower distortions observed in the numerical simulation results are attributed to the numerical model limitations. The numerical model currently does not consider the stress relaxation phenomena, which reduces the residual stress, and ultimately, the shrinkages are over-predicted. In the case of warpages/distortions, the numerical model assumes the perfect build plate adhesion, resulting in lower distortions; however, during the 3DP process, the imperfect build plate adhesion results in higher warpages. It is concluded that optimum dimensional control was achieved for PA6-CF material with a rectangular infill pattern fabricated at 0.100 mm of layer height. Generally, better mechanical properties (Young's modulus, yield stress, and maximum stress) were achieved for ABS material; however, PA6 material revealed higher yield strain. The effect of the infill pattern was not found to be very impactful on the mechanical properties of all the materials and layer heights. 3D-printed specimens revealed that the maximum Young's modulus was achieved for ABS material with a

hexagonal infill pattern fabricated at 0.125 mm of layer height. Similar trends were observed for the yield strength and maximum stress, except for the strain at yield. A maximum strain at yield was observed for PA6 material for rectangular and hexagonal infill patterns fabricated at layer heights of 0.100 mm or 0.125 mm. From the results, it is concluded that the numerical model could predict the FFF process-induced defects (shrinkages and distortions) effectively, as validated by the experimental results. Although within the acceptable range, variations were observed between the numerical model and 3D-printed specimens due to numerical model limitations, which will be addressed in future studies. In addition, further material models must be developed to adopt the numerical models for broader applications.

Data availability

The raw/processed data required to reproduce these findings cannot be shared at this time as the data also forms part of an ongoing study.

CRediT authorship contribution statement

Ans Al Rashid: Writing – original draft, Visualization, Validation, Software, Methodology, Investigation, Formal analysis, Data curation, Conceptualization, Writing – review & editing. **Shoukat Alim Khan:** Writing – review & editing, Visualization, Validation, Formal analysis. **Muammer Koç:** Writing – review & editing, Supervision, Resources, Project administration, Funding acquisition.

Declaration of competing interest

The authors declare that they have no known competing financial interests or personal relationships that could have appeared to influence the work reported in this paper.

Acknowledgements

None.

Appendix

Tables

Table A1
Dimensional Analysis of numerical model (NM) predictions and 3D-printed (3DP) Specimens

DOE	Analysis	Overall Length (mm)	Grip Width (mm)	Gauge Width (mm)	Thickness (mm)	Warpage (mm)
1	NM	164.86 ± 0.01	18.86 ± 0.01	12.92 ± 0.01	3.96 ± 0.01	0.11 ± 0.01
	3DP	164.95 ± 0.05	18.97 ± 0.02	12.99 ± 0.02	3.99 ± 0.01	0.13 ± 0.01
2	NM	164.69 ± 0.01	18.83 ± 0.01	12.86 ± 0.01	3.94 ± 0.01	0.12 ± 0.01
	3DP	164.92 ± 0.05	18.96 ± 0.02	12.97 ± 0.02	3.99 ± 0.01	0.15 ± 0.01
3	NM	164.65 ± 0.01	18.76 ± 0.01	12.78 ± 0.01	3.89 ± 0.01	0.15 ± 0.01
	3DP	164.85 ± 0.05	18.91 ± 0.02	12.93 ± 0.02	3.96 ± 0.01	0.18 ± 0.01
4	NM	164.35 ± 0.01	18.65 ± 0.01	12.63 ± 0.01	3.74 ± 0.01	0.33 ± 0.01
	3DP	164.49 ± 0.05	18.78 ± 0.02	12.75 ± 0.02	3.79 ± 0.01	0.39 ± 0.01
5	NM	164.12 ± 0.01	18.55 ± 0.01	12.52 ± 0.01	3.65 ± 0.01	0.34 ± 0.01
	3DP	164.33 ± 0.05	18.69 ± 0.02	12.68 ± 0.02	3.72 ± 0.01	0.46 ± 0.01
6	NM	164.45 ± 0.01	18.75 ± 0.01	12.72 ± 0.01	3.81 ± 0.01	0.32 ± 0.01
	3DP	164.56 ± 0.05	18.84 ± 0.02	12.83 ± 0.02	3.85 ± 0.01	0.35 ± 0.01
7	NM	164.38 ± 0.01	18.65 ± 0.01	12.66 ± 0.01	3.78 ± 0.01	0.24 ± 0.01
	3DP	164.60 ± 0.05	18.81 ± 0.02	12.81 ± 0.02	3.84 ± 0.01	0.28 ± 0.01
8	NM	164.68 ± 0.01	18.78 ± 0.01	12.80 ± 0.01	3.88 ± 0.01	0.19 ± 0.01
	3DP	164.77 ± 0.05	18.91 ± 0.02	12.92 ± 0.02	3.92 ± 0.01	0.22 ± 0.01
9	NM	164.56 ± 0.01	18.73 ± 0.01	12.74 ± 0.01	3.83 ± 0.01	0.25 ± 0.01
	3DP	164.70 ± 0.05	18.87 ± 0.02	12.86 ± 0.02	3.89 ± 0.01	0.28 ± 0.01

Table A2
Mechanical Performance using numerical model (NM) predictions and 3D-printed (3DP) Specimens

DOE	Analysis	Young's Modulus (MPa)	Yield Strength (MPa)	Strain At Yield	Maximum Stress (MPa)
1	NM	637.28	5.66	0.011	16.03
	3DP	354.88 ± 5	5.08 ± 0.5	0.016 ± 0.001	15.48 ± 0.2
2	NM	613.72	5.64	0.010	14.46
	3DP	481.37 ± 5	5.40 ± 0.5	0.013 ± 0.001	14.53 ± 0.2
3	NM	353.31	4.86	0.015	13.12
	3DP	278.64 ± 5	4.04 ± 0.5	0.016 ± 0.001	11.62 ± 0.2
4	NM	207.89	4.56	0.024	9.28
	3DP	156.91 ± 5	2.94 ± 0.5	0.020 ± 0.001	8.43 ± 0.2
5	NM	205.63	4.40	0.023	8.96
	3DP	145.62 ± 5	2.51 ± 0.5	0.019 ± 0.001	7.02 ± 0.2
6	NM	202.65	4.39	0.024	8.90
	3DP	165.59 ± 5	2.97 ± 0.5	0.020 ± 0.001	8.39 ± 0.2
7	NM	897.85	10.40	0.014	17.77
	3DP	904.34 ± 5	6.47 ± 0.5	0.009 ± 0.001	15.02 ± 0.2
8	NM	891.23	10.60	0.013	17.35
	3DP	1088 ± 5	6.31 ± 0.5	0.008 ± 0.001	15.20 ± 0.2
9	NM	896.96	10.65	0.014	17.46
	3DP	1119 ± 5	7.28 ± 0.5	0.008 ± 0.001	15.94 ± 0.2

References

- [1] T.A. Osswald, D. Jack, M.S. Thompson, Polymer composites: additive manufacturing of composites, *Polym. Compos.* 43 (6) (2022) 3496–3497, <https://doi.org/10.1002/pc.26631>.
- [2] A. Al Rashid, W. Ahmed, M.Y. Khalid, M. Koç, Vat photopolymerization of polymers and polymer composites: processes and applications, *Addit. Manuf.* 47 (Nov. 2021) 102279, <https://doi.org/10.1016/j.addma.2021.102279>.
- [3] J. Saroia, et al., A review on 3D printed matrix polymer composites: its potential and future challenges, *Int. J. Adv. Manuf. Technol.* 106 (5–6) (2020) 1695–1721, <https://doi.org/10.1007/s00170-019-04534-z>.
- [4] Z.U. Arif, M.Y. Khalid, A. Zolfagharian, M. Bodaghi, 4D bioprinting of smart polymers for biomedical applications: recent progress, challenges, and future perspectives, *React. Funct. Polym.* 179 (2022), <https://doi.org/10.1016/j.reactfunctpolym.2022.105374>. Elsevier B.V., Oct. 01.
- [5] H. Ikram, A. Al Rashid, M. Koç, Additive manufacturing of smart polymeric composites: literature review and future perspectives, *Polym. Compos.* (Aug. 2022), <https://doi.org/10.1002/pc.26948>.
- [6] B. Shaqour, et al., Gaining a better understanding of the extrusion process in fused filament fabrication 3D printing: a review, *Int. J. Adv. Manuf. Technol.* 114 (5–6) (2021) 1279–1291, <https://doi.org/10.1007/s00170-021-06918-6>.
- [7] B. Brenken, E. Barocio, A. Favaloro, V. Kunc, R.B. Pipes, Fused filament fabrication of fiber-reinforced polymers: a review, *Addit. Manuf.* 21 (October 2017) (2018) 1–16, <https://doi.org/10.1016/j.addma.2018.01.002>.
- [8] R. Imran, A. Al Rashid, M. Koç, Review on computational modeling for the property, process, product and performance (PPPP) characteristics of additively manufactured porous magnesium implants, *Bioprinting* 28 (Dec. 2022) e00236, <https://doi.org/10.1016/j.bprint.2022.e00236>.
- [9] N. Vidakis, M. Petousis, A. Maniadi, E. Koudoumas, A. Vairis, J. Kechagias, Sustainable additive manufacturing: mechanical response of acrylonitrile-butadiene-styrene over multiple recycling processes, *Sustainability* 12 (9) (May 2020), <https://doi.org/10.3390/SU12093568>.
- [10] N. Vidakis, et al., Medical-grade polyamide 12 nanocomposite materials for enhanced mechanical and antibacterial performance in 3D printing applications, *Polymers* 14 (3) (Feb. 2022), <https://doi.org/10.3390/polym14030440>.
- [11] N. Vidakis, et al., Polyethylene glycol and polyvinylpyrrolidone reduction agents for medical grade polyamide 12/silver nanocomposites development for material extrusion 3D printing: rheological, thermomechanical, and biocidal performance, *React. Funct. Polym.* 190 (2023) 105623, <https://doi.org/10.1016/j.reactfunctpolym.2023.105623>.
- [12] C. David, et al., Operational performance and energy efficiency of MEX 3D printing with polyamide 6 (PA6): multi-objective optimization of seven control settings supported by L27 Robust design, *Appl. Sci.* 13 (15) (Aug. 2023), <https://doi.org/10.3390/app13158819>.
- [13] M. Petousis, N. Vidakis, N. Mountakis, E. Karapidakis, A. Moutsopoulou, Compressive response versus power consumption of acrylonitrile butadiene styrene in material extrusion additive manufacturing: the impact of seven critical control parameters, *Int. J. Adv. Manuf. Technol.* 126 (3–4) (May 2023) 1233–1245, <https://doi.org/10.1007/s00170-023-11202-w>.
- [14] N. Vidakis, M. Petousis, E. Velidakis, M. Liebscher, V. Mechtcherine, L. Tzounis, On the strain rate sensitivity of fused filament fabrication (FFF) processed pla, abs, petg, pa6, and pp thermoplastic polymers, *Polymers* 12 (12) (Dec. 2020) 1–15, <https://doi.org/10.3390/polym12122924>.
- [15] N. Vidakis, et al., Multi-functional polyamide 12 (PA12)/multiwall carbon nanotube 3D printed nanocomposites with enhanced mechanical and electrical properties, *Adv. Compos. Mater.* 31 (6) (2022) 630–654, <https://doi.org/10.1080/09243046.2022.2076019>.
- [16] J. Ramian, J. Ramian, D. Dziob, Thermal deformations of thermoplast during 3D printing: warping in the case of ABS, *Materials* 14 (22) (Nov. 2021), <https://doi.org/10.3390/ma14227070>.
- [17] N. Yu, X. Sun, Z. Wang, D. Zhang, J. Li, Effects of auxiliary heat on warpage and mechanical properties in carbon fiber/ABS composite manufactured by fused deposition modeling, *Mater. Des.* 195 (2020) 108978, <https://doi.org/10.1016/j.matdes.2020.108978>.
- [18] N. Vidakis, C. David, M. Petousis, D. Sagris, N. Mountakis, Optimization of key quality indicators in material extrusion 3D printing of acrylonitrile butadiene styrene: the impact of critical process control parameters on the surface roughness, dimensional accuracy, and porosity, *Mater. Today Commun.* 34 (2023) 105171, <https://doi.org/10.1016/j.mtcomm.2022.105171>.
- [19] N. Vidakis, C. David, M. Petousis, D. Sagris, N. Mountakis, A. Moutsopoulou, The effect of six key process control parameters on the surface roughness, dimensional accuracy, and porosity in material extrusion 3D printing of polylactic acid: prediction models and optimization supported by robust design analysis, *Advances in Industrial and Manufacturing Engineering* 5 (2022) 100104, <https://doi.org/10.1016/j.aime.2022.100104>.
- [20] A. Al Rashid, S. Abdul Qadir, M. Koç, Microscopic analysis on dimensional capability of fused filament fabrication three-dimensional printing process, *J. Elastomers Plast.* 0 (0) (2021) 009524432110472, <https://doi.org/10.1177/00952443211047263>.
- [21] A. Al Rashid, H. Ikram, M. Koç, Additive manufacturing and mechanical performance of carbon fiber reinforced Polyamide-6 composites, *Mater. Today Proc.* 62 (12) (2022) 6359–6363, <https://doi.org/10.1016/j.matpr.2022.03.339>.
- [22] H. Kim, C.W. Macosko, Processing-property relationships of polycarbonate/graphene composites, *Polymer* 50 (15) (2009) 3797–3809, <https://doi.org/10.1016/j.polymer.2009.05.038>.
- [23] N. Mosleh, A.M. Rezadoust, S. Dariushi, Determining process-window for manufacturing of continuous carbon fiber-reinforced composite Using 3D-printing, *Mater. Manuf. Process.* 36 (4) (2021) 409–418, <https://doi.org/10.1080/10426914.2020.1843664>.
- [24] L. Fang, Y. Yan, O. Agarwal, J.E. Seppala, K.J. Hemker, S.H. Kang, Processing-structure-property relationships of bisphenol-A-polycarbonate samples prepared by fused filament fabrication, *Addit. Manuf.* 35 (April) (2020) 101285, <https://doi.org/10.1016/j.addma.2020.101285>.
- [25] M. Roy, O. Wodo, Data-driven modeling of thermal history in additive manufacturing, *Addit. Manuf.* 32 (December 2019) (2020) 101017, <https://doi.org/10.1016/j.addma.2019.101017>.
- [26] A. Lepoivre, N. Boyard, A. Levy, V. Sobotka, Heat transfer and adhesion study for the FFF additive manufacturing process, *Procedia Manuf.* 47 (2019) (2020) 948–955, <https://doi.org/10.1016/j.promfg.2020.04.291>.
- [27] T. D'Amico, A.M. Peterson, Bead parameterization of desktop and room-scale material extrusion additive manufacturing: how print speed and thermal properties affect heat transfer, *Addit. Manuf.* 34 (April) (2020) 101239, <https://doi.org/10.1016/j.addma.2020.101239>.
- [28] L. Wang, X. Chen, S. Kang, X. Deng, R. Jin, Meta-modeling of high-fidelity FEA simulation for efficient product and process design in additive manufacturing, *Addit. Manuf.* 35 (March) (2020) 101211, <https://doi.org/10.1016/j.addma.2020.101211>.
- [29] S.F. Costa, F.M. Duarte, J.A. Covas, Thermal conditions affecting heat transfer in FDM/FFE: a contribution towards the numerical modelling of the process, *Virtual Phys. Prototyp.* 10 (1) (2015) 35–46, <https://doi.org/10.1080/17452759.2014.984042>.
- [30] R. Comminal, M.P. Serdeczny, D.B. Pedersen, J. Spangenberg, Numerical modeling of the strand deposition flow in extrusion-based additive manufacturing, *Addit. Manuf.* 20 (2018) 68–76, <https://doi.org/10.1016/j.addma.2017.12.013>.

- [31] M.P. Serdeczny, R. Comminal, M.T. Mollah, D.B. Pedersen, J. Spangenberg, Numerical modeling of the polymer flow through the hot-end in filament-based material extrusion additive manufacturing, *Addit. Manuf.* 36 (July) (2020) 101454, <https://doi.org/10.1016/j.addma.2020.101454>.
- [32] S.F. Costa, F.M. Duarte, J.A. Covas, Estimation of filament temperature and adhesion development in fused deposition techniques, *J. Mater. Process. Technol.* 245 (2017) 167–179, <https://doi.org/10.1016/j.jmatprotec.2017.02.026>.
- [33] D.D. Phan, J.S. Horner, Z.R. Swain, A.N. Beris, M.E. Mackay, Computational fluid dynamics simulation of the melting process in the fused filament fabrication additive manufacturing technique, *Addit. Manuf.* 33 (January) (2020) 101161, <https://doi.org/10.1016/j.addma.2020.101161>.
- [34] A. D'Amico, A.M. Peterson, An adaptable FEA simulation of material extrusion additive manufacturing heat transfer in 3D, *Addit. Manuf.* 21 (February) (2018) 422–430, <https://doi.org/10.1016/j.addma.2018.02.021>.
- [35] F. Pigeonneau, D. Xu, M. Vincent, J.F. Agassant, Heating and flow computations of an amorphous polymer in the liquefier of a material extrusion 3D printer, *Addit. Manuf.* 32 (December 2019) (2020), <https://doi.org/10.1016/j.addma.2019.101001>.
- [36] R. Comminal, M.P. Serdeczny, D.B. Pedersen, J. Spangenberg, Motion planning and numerical simulation of material deposition at corners in extrusion additive manufacturing, *Addit. Manuf.* 29 (December 2018) (2019) 100753, <https://doi.org/10.1016/j.addma.2019.06.005>.
- [37] S. Tabacu, C. Ducu, Numerical investigations of 3D printed structures under compressive loads using damage and fracture criterion: experiments, parameter identification, and validation, *Extreme Mech Lett* 39 (2020) 100775, <https://doi.org/10.1016/j.eml.2020.100775>.
- [38] S. Hasanov, A. Gupta, A. Nasirov, I. Fidan, Mechanical characterization of functionally graded materials produced by the fused filament fabrication process, *J. Manuf. Process.* 58 (September) (2020) 923–935, <https://doi.org/10.1016/j.jmapro.2020.09.011>.
- [39] T. Webbe Kerekes, H. Lim, W.Y. Joe, G.J. Yun, Characterization of process–deformation/damage property relationship of fused deposition modeling (FDM) 3D-printed specimens, *Addit. Manuf.* 25 (December 2018) (2019) 532–544, <https://doi.org/10.1016/j.addma.2018.11.008>.
- [40] R. Ghandriz, K. Hart, J. Li, Extended finite element method (XFEM) modeling of fracture in additively manufactured polymers, *Addit. Manuf.* 31 (May 2019) 2020, <https://doi.org/10.1016/j.addma.2019.100945>.
- [41] A.A. Soufivand, N. Abolfathi, S.A. Hashemi, S.J. Lee, Prediction of mechanical behavior of 3D bioprinted tissue-engineered scaffolds using finite element method (FEM) analysis, *Addit. Manuf.* 33 (March) (2020), <https://doi.org/10.1016/j.addma.2020.101181>.
- [42] A. Al Rashid, M. Koç, Numerical predictions and experimental validation on the effect of material properties in filament material extrusion, *J. Manuf. Process.* 94 (May 2023) 403–412, <https://doi.org/10.1016/j.jmapro.2023.03.027>.
- [43] A. Al Rashid, M. Koç, Experimental validation of numerical model for thermomechanical performance of material extrusion additive manufacturing process: effect of process parameters, *Polymers* 14 (17) (Aug. 2022) 3482, <https://doi.org/10.3390/polym14173482>.
- [44] A. Al Rashid, M. Koç, Numerical simulations on thermomechanical performance of 3D printed chopped carbon fiber-reinforced polyamide-6 composites: effect of infill design, *J. Appl. Polym. Sci.* (Aug. 2022), <https://doi.org/10.1002/app.53081>.
- [45] A. Al Rashid, M. Koç, Experimental validation of numerical model for thermomechanical performance of material extrusion additive manufacturing process: effect of infill design & density, *Results in Engineering* (2022) 100860, <https://doi.org/10.1016/j.rineng.2022.100860>.
- [46] ASTM D638-14, in: Standard test method for tensile properties of plastics 1, 2006, pp. 1–15, <https://doi.org/10.1520/D0638-14.1>, January 2004.
- [47] Markforged, "Markforged." [Online]. Available: <https://markforged.com/>.
- [48] A. Al Rashid, M. Koc, Creep and recovery behavior of continuous fiber-reinforced 3DP composites, *Polymers* 13 (10) (May 2021) 1644, <https://doi.org/10.3390/POLYM13101644>, 2021, Vol. 13, Page 1644.
- [49] V. Durga Prasada Rao, P. Rajiv, V. Navya Geethika, Effect of fused deposition modelling (FDM) process parameters on tensile strength of carbon fibre PLA, *Mater. Today Proc.* 18 (2019) 2012–2018, <https://doi.org/10.1016/j.matpr.2019.06.009>.
- [50] U.K. uz Zaman, E. Boesch, A. Siadat, M. Rivette, A.A. Baqai, Impact of fused deposition modeling (FDM) process parameters on strength of built parts using Taguchi's design of experiments, *Int. J. Adv. Manuf. Technol.* 101 (5–8) (2019) 1215–1226, <https://doi.org/10.1007/s00170-018-3014-6>.
- [51] C. Abeykoon, P. Sri-Amphorn, A. Fernando, Optimization of fused deposition modeling parameters for improved PLA and ABS 3D printed structures, *International Journal of Lightweight Materials and Manufacture* 3 (3) (2020) 284–297, <https://doi.org/10.1016/j.ijlmm.2020.03.003>.
- [52] P. Kiss, J. Glinz, W. Stadlbauer, C. Burgstaller, V.M. Archodoulaki, The effect of thermally desized carbon fibre reinforcement on the flexural and impact properties of PA6, PPS and PEEK composite laminates: a comparative study, *Compos. B Eng.* 215 (Jun. 2021) 108844, <https://doi.org/10.1016/j.COMPOSITESB.2021.108844>.
- [53] A. Al Rashid, H. Ikram, M. Koç, Effect of carbon fiber reinforcement on dimensional variations of 3D printed polyamide-6 composites: a simulation study, *Turk. J. Chem.* 47 (1) (Jan. 2023) 33–39, <https://doi.org/10.55730/1300-0527.3513>.
- [54] W.Z. Nie, J. Li, Y.F. Zhang, in: Tensile properties of surface treated carbon fibre reinforced ABS/PA6 composites 39, Feb. 2013, pp. 16–20, <https://doi.org/10.1179/174328910X12608851832173>.